NANO LETTERS

2004
Vol. 4, No. 5
875−880

Anisotropic Diffusion in Face-Centered Cubic Opals

Michael R. Newton,[†] Kathleen A. Morey,[†] Yanhui Zhang,[†] Ryan J. Snow,[‡] Mohit Diwekar,[‡] Jing Shi,*[,‡] and Henry S. White*[,†]

Departments of Chemistry and Physics, University of Utah, Salt Lake City, Utah 84112

Received February 18, 2004; Revised Manuscript Received March 18, 2004

ABSTRACT

Diffusion in face-centered cubic (fcc) opals synthesized from 250 nm-diameter silica spheres was investigated by electrochemical methods and finite-element simulations. Opal modified electrodes (OME) ((111) opal surface orientation) were prepared by thermal evaporation of Au onto ∼1 mm-thick opals. Linear sweep voltammetry of Au OMEs in aqueous solutions containing an electroactive molecule and a supporting electrolyte (0.1 M Na_2SO_4) was used to determine molecular diffusion coefficients, D_{fcc}, within the opal. D_{fcc} is related to the diffusion coefficient of the molecule in free solution, D_{sol}, by the relationship D_{fcc}, $= (\epsilon/\tau)D_{sol}$, where ϵ is the interstitial volume fraction of a fcc opal ($\epsilon = 0.260$ for an infinitely thick opal) and τ is the tortuosity; the tortuosity reflects the increased distance traversed by molecules as they diffuse through the curved interstitial spaces of the opal lattice, and is a function of both the direction of transport relative to the lattice and the number of layers of spheres in the opal lattice. Finite-element simulations are used to compute τ for transport orthogonal to the (111), (110), and (100) surface orientations for 1–7 layers of spheres. Values of $\tau = 1.9 \pm 0.7$ and 3.1 ± 1.2 were obtained from experiment for transport of $Ru(NH)_6^{3+}$ and $Fe(CN)_6^{4-}$ normal to the (111) surface, respectively, in reasonable agreement with a value of ∼3.0 obtained from the simulation.

Introduction. The recent interest in opals comprising a close-packed face center cubic (fcc) lattice of spheres (typically SiO_2 or polystyrene of submicrometer radius) is due, in part, to their application in the synthesis of photonic crystals,[1−10] energy storage media,[11−14] novel magnetic materials,[15−17] and sensors.[18] These materials are typically prepared by infusion or diffusional transport of precursor species through the opal lattice, followed by removal of the spheres to create an inverted opal structure.[1,18−37]

Molecular transport occurs within the tortuous interstitial spaces of the opal, Figure 1. Based on geometric factors alone, the effective diffusivity of molecules within the fcc lattice of spheres, D_{fcc}, can be related to the diffusivitiy of molecules in free space, D_{sol}, by eq 1:

$$D_{fcc} = (\epsilon/\tau)D_{sol} \quad (1)$$

where ϵ is the void fraction (0.260 for infinite fcc lattice of close-packed spheres[38]) and τ represents the tortuosity.[39] The tortuosity accounts for the meandering path around the spheres that molecules take in diffusing through the opal.

Tortuosities of disordered materials are usually determined empirically.[40,41] Transport in ordered materials, such as opals, is more amendable to theoretical treatments and has been the subject of numerous investigations over the past century.[39,42−45] Maxwell first considered the electrical conductivity of composite materials comprising spherical particles randomly distributed in a continuum medium. The expression he derived for the effective isotropic electrical conductivity of a "dilute" system applies equally well to molecular diffusion.[42] A dilute system is one in which the

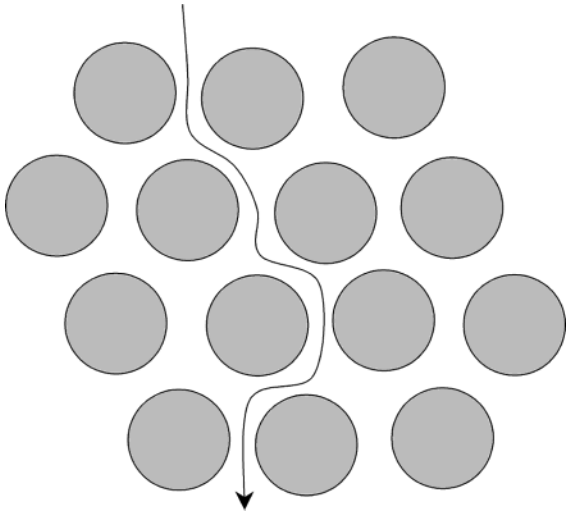

Figure 1. Schematic depicting diffusion through the interstitial region of a regular array of spheres. The spheres touch one another in a close-packed fcc opal.

* Corresponding authors: Email: jshi@physics.utah.edu; white@chem.utah.edu.
[†] Department of Chemistry.
[‡] Department of Physics.

10.1021/nl049729m CCC: $27.50
Published on Web 04/10/2004

volume fraction of spheres is small, and the particles are considered to be noninteracting. The effective diffusivity of such a composite is expressed in terms of the molecular diffusivities within the spheres (D_{sph}) and the medium (D_{sol}), and ϵ. Brenner and co-workers considered transport through a medium in which sphere particles are arranged on a periodic cubic lattice (simple, face-centered, and body center cubic), and also presented analytical expressions for dilute systems.[46,47] Keller considered the conductivity of an array of perfectly conducting ($D_{sph} = \infty$) spheres densely packed on a simple cubic lattice.[48] However, an expression for conduction in an array of densely packed insulating spheres ($D_{sph} = 0$) does not appear to have been reported. This latter situation corresponds to transport in opals.

In the present report, we examine diffusional transport in a fcc lattice of insulating spheres ($D_{sph} = 0$) in the close-packed limit. Values of D_{fcc} and τ for opals prepared from 250-nm diameter SiO_2 spheres are measured by electrochemical measurements and compared to values computed by finite element methods. An interesting part of this study, and distinct from the prior results for dilute systems, is the fact that diffusion in close-packed structures is anisotropic due to differences in the lengths of the paths that molecules follow in diffusing in different crystallographic directions. This anisotropy in dense arrays was anticipated by Maxwell, who wrote[49] "...certain systems of arrangements of the spheres causes the resistance of the compound medium to be different in different directions". Values of τ for diffusion normal to the three low index faces of a fcc crystal ((111), (100), and (110)) are presented. We also examine how τ and ϵ depend on the number of layers of spheres within the opal. Our results apply equally well to diffusion in gas or liquid phase, as well as to thermal and electronic conduction in fcc close-packed lattices comprising perfectly insulating spheres.

Experimental Section. Opals were synthesized by gravitational sedimentation of an aqueous suspension of 250 nm diameter silica spheres (with ~5% size distribution). The silica spheres were prepared from tetraethyl orthosilicate (TEOS) using standard growth techniques.[50,51] After four weeks of sedimentation into packed lattices, the opals were sintered at ~900 °C, yielding samples with a shiny opalescent surface that were mechanically robust and between 0.38 and 1.12 mm in thickness. Scanning electron microscopy images of an opal from this study are shown in Figure 2. While a hexagonal arrangement of spheres is the predominant structure, consistent with the (111) surface of a fcc lattice, occasional defects, such as those apparent in Figure 2b, were observed. The defects are a probable source of uncertainty in determining transport parameters, as they allow molecules to move more freely through the fcc lattice.

The opal-modified electrodes (OME) were prepared by sputter deposition of ~0.5 μm thick Au layer on one side of the opal. A Cu wire was attached to the Au coated side using Ag epoxy. The Cu wire, Au layer, and sides of the opal were coated with a thin layer of nail polish. The exposed areas of the Au OMEs were between 0.020 and 0.098 cm^2. Prior to electrochemical measurements, the electrodes were soaked in H_2O for 24 hours. A bare Au disk electrode (0.0199 cm^2, Bioanalytical Systems) was polished on a felt pad wetted with H_2O.

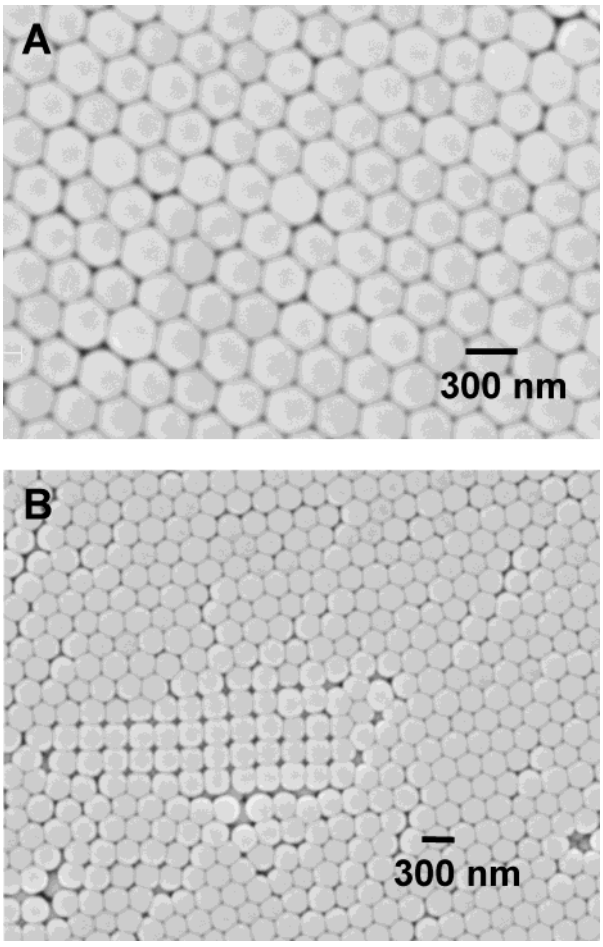

Figure 2. SEM images of an opal.

Voltammetric measurements were performed using a standard 3-electrode cell, employing a Ag/AgCl reference electrode and a Pt wire auxiliary electrode. All solutions were bubbled with N_2 to removed dissolved O_2. A Bioanalytical Systems, Inc. model CV-27 waveform generator and potentiostat was used to obtained voltammetric curves. Data were recorded on a PC using data acquisition programs written in Labview.

Potassium ferricyanide dihydrate, $K_4Fe(CN)_6(H_2O)_2$ (99%, Mallinckrodt), hexaaminеruthenium(III) chloride, $Ru(NH_3)_6Cl_3$ (99%, Strem Chemicals), and sodium sulfate, Na_2SO_4 (Mallinckrodt), were used as received. All solutions for the electrochemical measurements were prepared using 18 MΩ·cm water obtained from a Barnstead "E-pure" water purification system.

Finite-element simulations of the flux through a closed pack fcc lattice of spheres were performed using Femlab 2.0 software (Comsol, Inc.) operated on a Dell Dimension XP (Pentium 4 CPU, 3.2 GHz, 2 GB RAM). Finite-difference simulations of voltammetric experiments were performed using DigiSim 3 (Bioanalytical Systems, Inc.).

Results and Discussion. *Voltammetric Measurement of Opal Tortuosity Normal to the (111) Surface.* Figure 3 shows

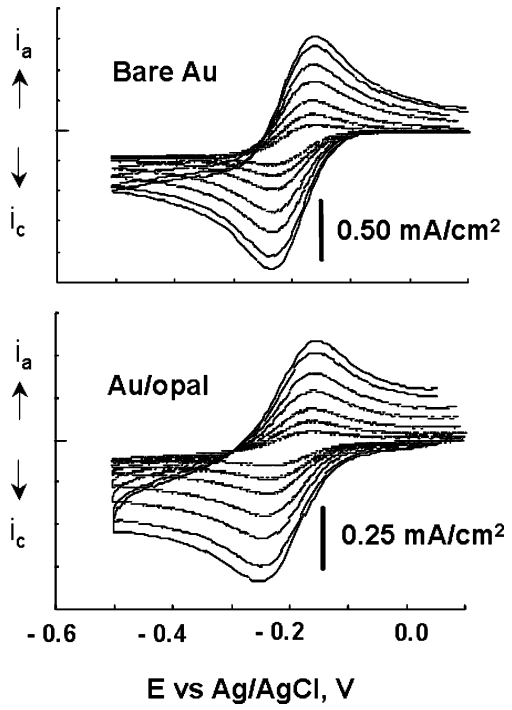

Figure 3. Cyclic voltammetric responses of (top) a bare Au electrode, and (bottom) a Au OME electrode in an O_2-purged, unstirred, aqueous solution containing 4.99 mM $Ru(NH_3)_6Cl_3$ and 0.10 M Na_2SO_4. The curves correspond to scan rates of 4, 8, 15, 30, 50, 80, and 100 mV/s. All scans were initiated at 0.1 V in the negative direction.

the voltammetric response of a bare Au electrode (0.0199 cm^2) and a Au OME (0.0571 cm^2) in a solution containing 4.99 mM $Ru(NH)_6^{3+}$ and 0.10 M Na_2SO_4 as the supporting electrolyte. The voltammetric response for each electrode corresponds to the reversible 1 e^- reduction of $Ru(NH)_6^{3+}$, eq 2. The peak-shaped voltammograms observed at

$$Ru(NH_3)_6^{3+} + e^- \rightleftharpoons Ru(NH_3)_6^{2+} \qquad (2)$$

both the bare Au and Au OME electrode are indicative of an electrochemical reaction limited by diffusional transport of the reactant to the electrode surface. A slightly larger potential splitting between the cathodic and anodic peak currents for the OME reflects a larger ohmic potential drop ($= iR$) for this electrode, a consequence of the larger area of the OME, and, thus, larger current, i, as well as increased solution resistance, R, within the opal matrix relative to free solution. Larger peak splitting was observed for electrodes prepared from thicker opals.

The diffusion coefficient of $Ru(NH)_6^{3+}$ is readily obtained by measuring the voltammetric peak current density, i_p/A, as a function of scan rate, ν. For a diffusion controlled reaction, the value of i_p/A on the first scan is proportional to the square root of ν, eq 3,[52]

$$i_p/A = 0.4463nFC^* (nF/RT)^{1/2}\nu^{1/2}D^{1/2} \qquad (3)$$

where D represents either the diffusivity of $Ru(NH)_6^{3+}$

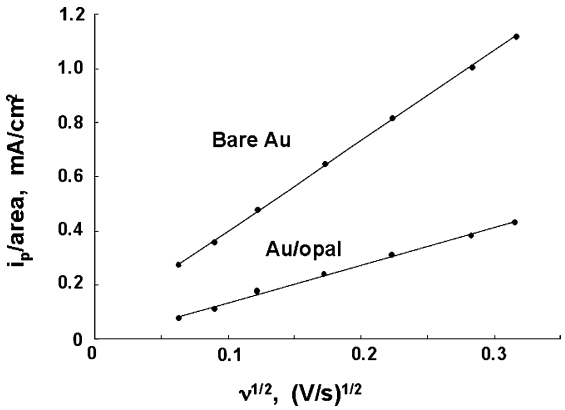

Figure 4. Plot of voltammetric peak current density (i_p/A) vs square root of the scan rate ($\nu^{1/2}$) for the voltammetric data presented in Figure 2.

measured using either the OME (D_{fcc}) or the bare electrode (D_{sol}), F is Faraday's constant, C^* is the bulk concentration of $Ru(NH)_6^{3+}$, n is the number of electrons transferred, A is the electrode area, R is the molar gas constant, and T is temperature. The slope of a plot of i_p/A vs. $\nu^{1/2}$ yields either D_{fcc} or D_{sol}.

Figure 4 shows a plot of i_p/A vs. $\nu^{1/2}$ for an Au OME (0.7 mm thick opal) and a bare Au electrode. As expected from eq 3, a linear dependence i_p/A vs. $\nu^{1/2}$ is obtained in both cases. Based on seven independent sets of measurements using different OMEs, we obtain $D_{fcc} = (8.30 \pm 2.96) \times 10^{-7}$ cm^2/s for $Ru(NH)_6^{3+}$ at the Au OME. The diffusivity of $Ru(NH)_6^{3+}$ in the bulk solution, D_{sol}, was found to be equal to $(6.1 \pm 0.2) \times 10^{-6}$ cm^2/s, in good agreement with values of D_{sol} for this molecule reported in the literature (e.g., 6.7×10^{-6} cm^2/s and 5.3×10^{-6} cm^2/s in aqueous 0.1 M sodium trifluoroacetate[53] and phosphate solutions,[54] respectively). It is important to note that the uncertainty in D_{fcc} is much larger than the uncertainty in D_{sol}. This difference almost certainly reflects differences in defect structure and density in the opals used to fabricate Au OMEs.

By rearrangement of eq 1, $\tau = \epsilon(D_{sol}/D_{fcc})$, where ϵ is equal to 0.260. From the values of D_{fcc} and D_{sol} reported above, we compute τ to be equal to 1.9 ± 0.7. The uncertainty in τ is largely due to the measurement of D_{fcc}.

A similar voltammetric analysis was performed using $Fe(CN)_6^{-4}$ as the redox active molecule. The electrochemical reaction corresponds to the 1 e^- oxidation of $Fe(CN)_6^{-4}$, which yields voltammetric results analogous to those shown in Figure 3. Values of $D_{fcc} = (4.7 \pm 1.9) \times 10^{-7}$ cm^2/s (3 independent measurements) and $D_{sol} = (5.6 \pm 0.2) \times 10^{-6}$ cm^2/s were obtained from linear plots of i_p/A vs. $\nu^{1/2}$. The latter value is in good agreement with the accepted literature value under slightly different solution conditions (6.5×10^{-6} cm^2/s in 0.1 M KCl[55]). From these values, τ is computed to be 3.1 ± 1.2.

We note that eq 3 is derived assuming a semi-infinite boundary condition, i.e., the diffusion layer that develops in front of the electrode is thin in comparison to the medium into which the molecules are diffusing. For voltammetric measurements using an OME, this assumption is only valid

if the diffusion layer is thin compared to the thickness of the opal. To check this assumption, a finite-difference simulation (DigiSim) was performed to compute the concentration profiles that develop inside the 0.7 mm thick opal during the voltammetric experiment. Based on the slowest scan rate employed in the above experiments, $\nu = 4$ mV/s, the measured value of D_{fcc} (1.2×10^{-6} cm^2/s), and arbitrarily defining the diffusion layer thickness as the point where the concentration of $Ru(NH)_6^{3+}$ is equal to 95% of its bulk value, the diffusion layer obtains a depth of ca. 0.1 mm when the peak current is observed and measured. Since the depletion layer is significantly less that the opal thickness, the requirement of a semi-infinite boundary is satisfied. The finding that the plot of i_p/A vs. $\nu^{1/2}$ is linear is consistent with this conclusion.

While the void fraction, ϵ, of a closed packed fcc lattice of spheres may be readily calculated from geometry to be 0.260, we also measured this value to ensure that our opals had the assumed geometry throughout the bulk of the crystal (since SEM images show only the geometric arrangement of the exposed opal surface). To measure ϵ, the mass of a sample of an opal was measured in air and after allowing it to soak overnight in H_2O. After carefully removing any excess water clinging to the opal surface, the difference in these masses is equal to $\epsilon V(\rho_{H_2O} - \rho_{air})$, where ρ_{H_2O} and ρ_{air} are the densities, respectively, of H_2O and air, and V is the sample volume. Analysis of three opals by this method yielded $\epsilon = 0.25$, 0.26, and 0.27 ± 0.03, in agreement with the theoretical value for an ideal fcc crystal.

Finite-Element Simulations of the Flux Across an Opal. For comparison to experiment, we also determined τ by finite element simulation of the steady-state molecular flux in a close-packed fcc lattice of spheres. The experiment described in the previous section corresponds to molecular transport normal to the (111) surface. However, as noted in the Introduction, diffusion in a closed-packed lattice of spheres is anisotropic. Thus, we performed simulations of diffusion normal to each of the low index planes.

The simulations were performed with the two opposing and parallel faces of the model opal exposed to 1 and 0 mM solutions of the diffusing molecule, respectively, to set up a driving force for diffusion. A zero-flux boundary condition was assumed on the remaining surfaces. The radius of the spheres comprising the opal was set equal to 300 nm, and the diffusivity of the molecule, D_{sol}, in free solution was assumed to be 10^{-6} cm^2/s.

The tortuosity and void fraction of a fcc close-packed lattice of spheres both depend on the number of layers of spheres, N, that make up the crystal. For an infinite fcc lattice of spheres, $\epsilon = 0.260$. For small values of N (<100), ϵ is a function of N as described below. The thicknesses of the opals used in our experiments are between 0.38 and 1.12 mm, corresponding approximately to N between 1500 and 6000, (i.e., an infinite lattice). Due to finite computational memory, our simulations were limited to $N = 1$ to 7.

Figure 5 shows the geometrical model used to simulate the flux normal to the (111) surface across an opal with $N = 3$. For the purpose of visualizing the concentration and flux distributions within the interstitial spaces, the solid spherical particles comprising the opal are omitted in Figure 4a and b, and are represented by open space. The hexagonal symmetry of the (111) plane allows the simulation to be performed in a cell with triangular cross-sectional area with apexes that are defined by the plane intersecting the bottom of the first layer of spheres (i.e., the A layer of the ABC fcc repeating structure). For an OME, this plane corresponds to the electrode surface in contact with the opal.

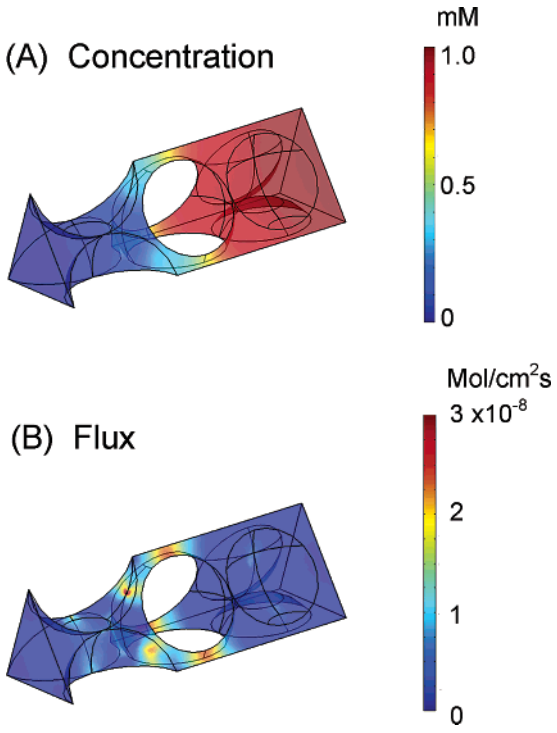

Figure 5. Concentration and flux distributions for diffusion normal to the (111) surface for an opal with $N = 3$. The open-spherical regions correspond to spherical particles. Simulation cells for transport normal to the (110) and (100) surfaces are presented in Supporting Information.

As expected, the concentration and flux profiles in Figure 5 clearly show that the molecular flux through the opal is limited by diffusion through the narrow interstitial regions. Similar simulations were performed for diffusion normal to the (110) and (100) planes with qualitatively similar results (see Supporting Information). The rate of transport (mol/s) across the simulation cell in the presence and absence of the spherical particles, R_{fcc} and R_{sol}, respectively, was computed by numerical integration of the flux across the cross-sectional surface at which the concentration is fixed at 0 mm (see Figure 5). The ratio R_{fcc}/R_{sol} is equal to D_{fcc}/D_{sol}, which is plotted in Figure 6 as a function of N and crystallographic orientation. Inspection of this plot shows that D_{fcc} for transport normal to the (111) surface is approximately twice as small as the corresponding values for transport normal to either the (110) or (100) directions. To determine whether the anisotropy in D_{fcc}/D_{sol} is due to variations in ϵ or in τ, we analytically computed ϵ over the same range of N. As shown in Figure 6b, values of ϵ depend on N but converge in all three directions to the theoretical

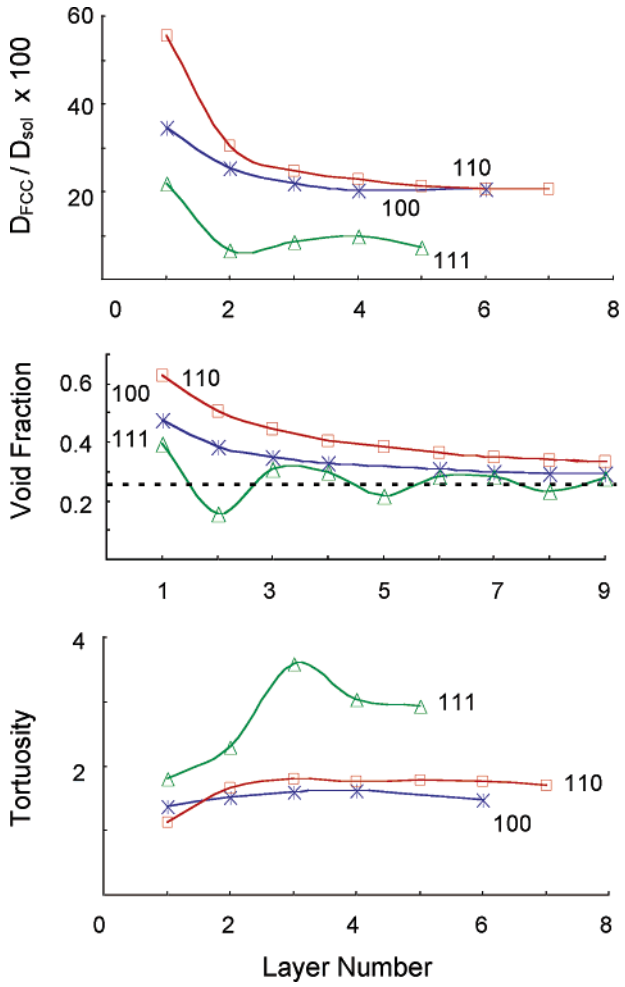

Figure 6. Dependence of (a) D_{fcc}/D_{sol}, (b) void faction (ϵ), and (c) tortuosity (τ) on the number of layers of spherical particles, N, and direction of transport normal to the planes indicated on the figure. Results from finite-element simulations.

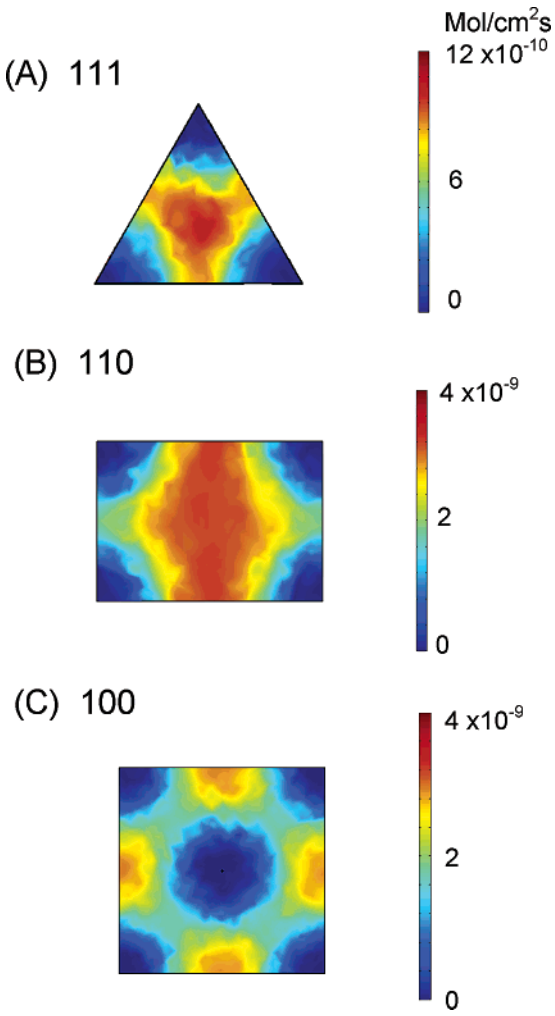

Figure 7. Flux distribution on an electrode surface in contact with (111), (110), and (100) opals. The triangle in (a) corresponds to the triangle at the left-hand side of the simulation cell in Figure 5.

infinite lattice value of 0.260 (for $N = 100$, $\epsilon = 0.261$, 0.267, and 0.263 in the (111), (110), and (100) directions).

The tortuosity was computed from eq 1 using values of D_{fcc}/D_{sol} and ϵ as a function of N. Note that because τ is based on the ratio D_{fcc}/D_{sol}, the numerical results are independent of the particle diameter, the bulk solution diffusivity D_{sol}, and the concentration difference (i.e., driving force) assumed in the simulation. We also note that D_{fcc} and D_{sol} reflect molecular properties and are independent of whether steady-state or transient transport is considered. Thus, τ obtained from the computer simulation of steady-state transport has the same physical meaning as τ determined from the transient voltammetric measurement.

The numerical results in Figure 6c indicate that τ has a strong dependence on crystallographic orientation, being approximately twice as large for transport normal to the (111) plane than the other two low-index planes. This anisotropy can be understood using a simple ball model of a fcc lattice, where it is readily observed that the interstitial spaces in the direction normal to the (111) surfaces are significantly more curved than those in the direction normal to the (110) and (100) planes. The maximum in τ that occurs at $N = 3$ is real and simply reflects a relatively longer average path length, a consequence of the fcc lattice structure. The value of $\tau = 3.0$ for transport normal to the (111) planes at $N = 5$ can be taken as an approximation of τ in this direction for an infinite crystal. Our experiments yield $\tau = 1.9 \pm 0.7$ for $Ru(NH_3)_6^{+3}$ and 3.1 ± 1.2 for $Fe(CN)_6^{-4}$, which are in reasonable agreement with this value. As previously noted, the large uncertainty in the experimental values of τ is due to variance in the defect structure and density in different opals used to fabricate the Au OMEs. Since the computed value of τ reflects only the arrangement of spheres in the opal, the agreement between theory and experiment suggests that $Ru(NH)_6^{3+}$ and $Fe(CN)_6^{-4}$ diffuse through the opal without interacting strongly with the surfaces of the silica spheres. This is somewhat surprising given the large difference in the electrical charge of these ions (+3 and −4) and the fact that the SiO_2 surface is negatively charged at the neutral pHs employed in these experiments.

Finally, Figure 7 shows the spatial distributions of the fluxes, J, across the planes defining the bottom surfaces of the simulation cells for transport normal to all three low-index directions. As noted above, this plane also corresponds to the electrode surface on which the opals are deposited. Since the flux is directly proportional to the current (i.e.,

$i/A = nFJ$), the distributions shown in Figure 7 also correspond to the current density on the electrode surface. It is clear the current is very nonuniformly distributed, a consequence of the large variation of the cross sectional area of the interstitial regions in the direction of diffusion.

Conclusions. Based on geometric factors alone, the rate of molecular transport normal to the (111) plane of a close-packed fcc lattice of spheres is ~10 times smaller relative to the free solution value. The tortuosity in the direction normal to the (111) plane is estimated to be ~3.0 based on finite element simulations. Voltammetric measurements of the diffusion coefficients of two electroactive molecules at Au OME and bare Au electrodes yield values of τ in reasonable agreement with the computed value.

Acknowledgment. This work was supported by the DoD Multidisciplinary University Research Initiative (MURI) program administered by the Office of Naval Research under Grant N00014-01-1-0757 and the Office of Naval Research, and NSF-NIRT Grant 0102964. K.A.M. was supported in part by a NSF-REU summer fellowship (CHE0097253). H.S.W. gratefully acknowledges helpful discussions with P. N. Bartlett (University of Southampton, UK), C. Amatore (Ecole Normale Supérieure), E. L. Cussler (U. Minnesota), and B. Dunn (UCLA) regarding OMEs and diffusion.

Supporting Information Available: Concentration and flux distributions for the (100) and (110) surfaces for opals with $N = 3$. This material is available free of charge via the Internet at http://pubs.acs.org.

References

(1) Norris, D. J.; Vlasov, Y. A. *Adv. Mater.* **2001**, *13*, 371.
(2) Rugge, A.; Becker, J. S.; Gordon, R. G.; Tolbert, S. H. *Nano Lett.* **2003**, *3*, 1293.
(3) Miguez, H.; Meseguer, F.; Lopez, C.; Holgado; M.; Andreasen, G.; Mifsud, A.; Fornes, V. *Langmuir* **2000**, *16*, 4405.
(4) King, J. S.; Neff, C. W.; Park, C. J.; Blomquist, S.; Forsythe, E.; Morton, D. *Appl. Phys. Lett.* **2003**, *83*, 2566.
(5) Subramanian, G.; Manoharan, V. N.; Thorne, J. D.; Pine, D. J. *Adv. Mater.* **1999**, *11*, 1261.
(6) Zahidov, A. A.; Baughman, R. H.; Iqbal, Z.; Cui, C.; Khayrullin, I. I.; Dantas, S. O.; Marti, J.; Ralchenko, V. G. *Science* **1998**, *282*, 897.
(7) Wijnhoven, J. F. G. J.; Vos, W. L. *Science* **1998**, *281*, 802.
(8) Bianco, A.; Chomski, E.; Grabtchak, S.; Ibisate, M.; John, S.; Leonard, S. W.; Lopez, C.; Mesequer, F.; Miguez, H.; Mondla, J. P.; Ozin, G. A.; Toader, O.; Van Driel, H. M. *Nature* **2000**, *405*, 437.
(9) Wang, C.; Caruso, F. *Adv. Mater.* **2001**, *13*, 350.
(10) See the special issue on photonic crystals. *Adv. Mater.* **2001**, *13*, 369.
(11) Stein, A.; Schroden, R. C. *Curr. Opin. Solid State Mater. Sci.* **2001**, *5*, 553.
(12) Sakamoto, J. S.; Dunn, B. *J. Mater. Chem.* **2002**, *12*, 2859.
(13) Stein, A. *Adv. Mater.* **2003**, *15*, 763.
(14) Kang, S.; Yu, J. S.; Kruk, M.; Jaroniec, M. *Chem. Commun.* **2002**, 1670.
(15) Bartlett, P. N.; Ghanem, M. A.; Hallag, E.; De Groot, P.; Zhukov, A. *J. Mater. Chem.* **2003**, *13*, 2596.
(16) Yan, H.; Blanford, C. F.; Smyrl, W. H.; Stein, A. *Chem. Commun.* **2000**, 1477.
(17) Xu, L.; Zhou, W. L.; Frommen, C.; Baughman, R. H.; Zakhidov, A. A.; Malkinski, L.; Wang, J. Q.; Wiley, J. B. *Chem. Commun.* **2000**, 997.
(18) Cassagneau, S.; Caruso, F. *Adv. Mater.* **2002**, *14*, 34.
(19) Rodriguez-Gonzalez, B.; Salgueirino-Maceira, V.; Garcia-Santamaria, F.; Liz-Marzan, L. M. *Nano Lett.* **2002**, *2*, 471.
(20) Yu, A.; Meiser, F.; Cassagneau, T.; Caruso, F. *Nano Lett.* **2003**, *4*, 177.
(21) Zeng, F.; Sun, Z.; Wang, C.; Ren, B.; Liu, X.; Tong, Z. *Langmuir* **2002**, *18*, 9116.
(22) Braun, P. V.; Witzius, P. *Nature* **1999**, *402*, 603.
(23) Ootake, R.; Takamoto, N.; Fujii, A.; Ozaki, M.; Yoshino, K. *Synth. Met.* **2003**, *137*, 1417.
(24) Bartlett, P. N.; Birkin, P. R.; Ghanem, M. A.; Toh, C.-S. *J. Mater. Chem.* **2001**, *11*, 849.
(25) Bartlett, P. N.; Baumberg, J. J.; Birkin, P. R.; Ghanem, M. A.; Netti, M. C. *Chem. Mater.* **2002**, *14*, 2199.
(26) Wijnhoven, J. F. G. J.; Zevenhuizen, S. J. M.; Hendriks, M. A.; Vanmaekelbergh, D.; Keller, J. J.; V., W. L. *Adv. Mater.* **2000**, *12*, 888.
(27) Xu, L.; Zhou, W.; Kozlov, M. E.; Khayrullin, I. I.; Udod, I.; Zahidov, A. A.; Baughman, R. H.; Wiley, J. B. *J. Am. Chem. Soc.* **2001**, *123*, 763.
(28) Takayuki, S.; Wada, Y.; Kitamura, T.; Shozo, Y. *Chem. Lett.* **2001**, *1*, 38.
(29) Misoska, V.; Price, W.; Ralph, S.; Wallace, G. *Synth. Met.* **2001**, *121*, 1501.
(30) Sumida, T.; Wada, Y.; Kitamura, T.; Takayuki, S.; Yanagida, S. *Langmuir* **2002**, *18*, 3886.
(31) Jiang, P.; Cizeron, J.; Bertone, J. F.; Colvin, V. L. *J. Am. Chem. Soc.* **1999**, *121*, 7957.
(32) Holland, B. T.; Abrams, L.; Stein, A. *J. Am. Chem. Soc.* **1999**, *121*, 4308.
(33) Lee, Y.-C.; Kuo, T.-J.; Hsu, C.-J.; S., Y. W.; Chen, C.-C. *Langmuir* **2002**, *18*, 9942.
(34) Yang, P.; Deng, T.; Zhao, D.; Feng, P.; Pine, D.; Chmelka, B. F.; Whitesides, G. M.; Stucky, G. D. *Science* **1998**, *282*, 2244.
(35) Johnson, S. A.; Ollivier, P. J.; Mallouk, T. E. *Science* **1999**, *283*, 963.
(36) Velev, O. D.; Jede, T. A.; Lobo, R. F.; Lenhoff, A. M. *Nature* **1997**, *389*, 447.
(37) Braun, P. V.; Wiltzius, P. *Nature* **1999**, *402*, 603.
(38) Kittel, C. *Introduction to Solid State Physics*, 5th ed.; John Wiley & Sons: New York, 1976.
(39) Cussler, E. L. *Diffusion*; Cambridge University Press: New York, 1997.
(40) Armatas, G. S.; Salmas, C. E.; Louloudi, M.; Androutsopoulos, G. P.; Pomonis, P. J. *Langmuir* **2003**, *19*, 3128.
(41) Satterfield, C. N. *Mass Transfer in Heterogeneous Catalysis*; MIT Press: Cambridge, MA, 1970.
(42) Maxwell, J. C. *Treatise on Electrochemistry and Magnetism*, 3rd ed.; Oxford University Press: 1892; Vol. 1.
(43) Crank, J. *The Mathematics of Diffusion*, 2nd ed.; Oxford University Press: New York, 1975.
(44) Mason, E. A.; Malinauskas, A. P. *Gas Transport in Porous Media: The Dusty-Gas Model*; Elsevier: Amsterdam, 1983.
(45) Carslaw, H. S.; Jaeger, J. C. *Heat Conduction in Solids*, 2nd ed.; Clarendon Press: Oxford, 1959.
(46) Zuzovsky, M.; Brenner, H. *J. Appl. Math. Phys.* **1977**, *28*, 979.
(47) Brenner, H.; Edwards, D. A. *Macrotransport Processes*; Butterworth-Heinemann: Boston, 1993.
(48) Keller, J. B. *J. Appl. Phys.* **1963**, *34*, 991.
(49) Maxwell, J. C. *Treatise on Electrochemistry and Magnetism*, 3rd ed.; Oxford University Press: 1892; Vol. 1., p 441.
(50) Stober, W.; Fink, A. *J. Colloid Interface Sci.* **1968**, *26*, 62.
(51) Bougush, G. H.; Tracy, M. A. *J. Non-Cryst. Solids* **1988**, *104*, 95.
(52) Bard, A. J.; Faulkner, L. R. *Electrochemical Methods: Fundamentals and Applications*, 2nd ed.; Wiley: New York, 2001.
(53) Wiph, D. O.; Kristensen, E. W.; Deakin, M. R.; Wightman, R. M. *Anal. Chem.* **1989**, *60*, 306.
(54) Wightman, R. M.; Wiph, D. O. *J. Electroanal. Chem.* **1989**, *15*, 267.
(55) von Stackelberg, M.; Pilgram, M.; Toome, Z. *Z. Elektrochem.* **1953**, *57*, 342.

NL049729M